

Virulence

ISSN: 2150-5594 (Print) 2150-5608 (Online) Journal homepage: www.tandfonline.com/journals/kvir20

Evolutionary adaptations in iron capture via type II pyoverdine in XDR *Pseudomonas aeruginosa ST235*

Cansel Vatansever , Ani Akpınar , Selin Kolsuz , Gulin Özcan , Güz Ekinci , Özlem Azap , Alp Eren Kazar , Kerem Kahraman , Emir Ural , Çağdaş Dağ , Mehmet Gönen & Fusun Can

To cite this article: Cansel Vatansever , Ani Akpınar , Selin Kolsuz , Gulin Özcan , Güz Ekinci , Özlem Azap , Alp Eren Kazar , Kerem Kahraman , Emir Ural , Çağdaş Dağ , Mehmet Gönen & Fusun Can (2026) Evolutionary adaptations in iron capture via type II pyoverdine in XDR *Pseudomonas aeruginosa ST235*, Virulence, 17:1, 2696664, DOI: 10.1080/21505594.2026.2696664

To link to this article: https://doi.org/10.1080/21505594.2026.2696664

© 2026 The Author(s). Published by Informa UK Limited, trading as Taylor & Francis Group.

View supplementary material

Published online: 13 Aug 2026.

Submit your article to this journal

Article views: 356

View related articles

View Crossmark data

Full Terms & Conditions of access and use can be found at
https://www.tandfonline.com/action/journalInformation?journalCode=kvir20

VIRULENCE
2026, VOL. 17, NO. 1, 2696664
https://doi.org/10.1080/21505594.2026.2696664

Taylor & Francis
by informa

PATHOGEN GENOMICS

OPEN ACCESS Check for updates

Evolutionary adaptations in iron capture via type II pyoverdine in XDR *Pseudomonas aeruginosa ST235*

Cansel Vatansever [a,b], Ani Akpınar [a], Selin Kolsuz [c], Gulin Özcan [b], Güz Ekinci [d], Özlem Azap [e], Alp Eren Kazar [f], Kerem Kahraman[f], Emir Ural[a], Çağdaş Dağ [f], Mehmet Gönen [a,g], and Fusun Can [a,b]

[a]Koç University İşBank Center for Infectious Diseases (KUISCID), Istanbul, Turkey; [b]Department of Medical Microbiology, School of Medicine, Koç University, Istanbul, Turkey; [c]Department of Medicine, Division of Gastroenterology and Hepatology, University of Illinois at Chicago, Chicago, IL USA; [d]Max-Planck Institute of Infection Biology, Berlin, Germany; [e]Department of Infectious Diseases and Clinical Microbiology, Faculty of Medicine, Başkent University, Ankara, Turkey; [f]Nanofabrication and Nanocharacterization Centre for Scientific and Technological Advanced Research, Koç University, Istanbul, Turkey; [g]Department of Industrial Engineering, College of Engineering, Koç University, Istanbul, Turkey

ABSTRACT

Pseudomonas aeruginosa ST235 is a globally disseminated, high-risk clone associated with multidrug resistance and increased virulence. This study explores structural and functional modifications in the pyoverdine synthesis system of the ST235 clone. We analysed extensively drug-resistant (XDR) *P. aeruginosa* isolates derived from invasive infections and identified a modified type II pyoverdine system unique to ST235. This system is characterized by a truncated *pvdS* gene and the presence of a novel GNAT-family N-acetyltransferase. Genomic analysis revealed significant rearrangements within the pyoverdine loci, including the replacement of the *pvdD–pvdJ–pvdI* gene cluster with two large non-ribosomal peptide synthetases and an alpha/beta-hydrolase. Additionally, multiple non-synonymous variations were identified in the *pvdA* and *pvdF* genes of ST235. Despite structural modifications within the pyoverdine biosynthetic locus, ST235 isolates exhibited higher overall pyoverdine production than non-ST235 strains. Moreover, iron titration assays confirmed the exceptionally strong Fe(III)-chelating activity of pyoverdine produced by ST235. Nuclear magnetic resonance (NMR) spectroscopy presented distinct chemical shifts in the pyoverdine molecule produced by ST235, particularly in the chromophore and ornithine regions. These findings indicate that the modified type II pyoverdine system of ST235 provides an evolutionary advantage by optimizing iron acquisition without additional metabolic costs, potentially contributing to the persistence and spread of the clone.

ARTICLE HISTORY
Received 7 November 2025
Revised 5 May 2026
Accepted 25 June 2026

KEYWORDS
P.aeruginosa; ST235 high risk clone; type II pyoverdine

Introduction

Pseudomonas aeruginosa is a ubiquitous opportunistic pathogen responsible for a wide range of human infections. The ST235 high-risk clone, which emerged in Europe and spread globally, is particularly concerning due to its enhanced virulence and increased ability to acquire mobile resistance elements [1–3]. The severe infections and high fatality rates associated with this clone underscore the urgent need for effective control strategies [2,3].

Pyoverdine, the primary siderophore of *P. aeruginosa*, plays a crucial role in iron acquisition and serves as a significant virulence factor [4]. Unlike most bacterial genomic regions, the pyoverdine locus exhibits remarkable sequence diversity within the core genome, indicative of intense positive selection [5]. This diversity is particularly noteworthy, contrasting with the typically infrequent positive selection observed in bacterial evolution. The amino acid sequence variability in bacterial proteins, including those involved in pyoverdine synthesis and uptake, often facilitates the evasion of host immune responses and defense mechanisms [5,6]. Modifications to the pyoverdine synthesis pathway or its receptors could profoundly impact *P. aeruginosa*'s survival and adaptation across diverse environments, including host tissues [7,8].

Three structurally distinct pyoverdine types (PVD-I, PVD-II, and PVD-III) have been identified, each with a unique peptide chain and a specific ferri-pyoverdine receptor (FpvAI, II, or III) [9,10] {Ringel, 2018 #329}. FpvB serves as a secondary receptor when ferripyoverdine levels are low or pyoverdine is in excess [11].

Pyoverdine biosynthesis involves a complex pathway beginning in the cytoplasm and concluding in the periplasm [12,13]. Key components include biosynthesis enzymes (PvdA, PvdF, PvdH) and nonribosomal peptide synthetases (NRPSs: PvdL, PvdI, PvdJ, PvdD) forming the "siderosome" (Figure 1). While most pyoverdine

CONTACT Fusun Can fucan@ku.edu.tr
Present affiliation for Selin Kolsuz is Department of Lymphoma & Myeloma, The University of Texas, MD Anderson Cancer Center, Houston, Texas, USA.
Present affiliation for Gulin Özcan is Department of Medical Microbiology, Faculty of Medicine, Atılım University, Ankara, Türkiye.
Supplemental data for this article can be accessed online at https://doi.org/10.1080/21505594.2026.2696664

© 2026 The Author(s). Published by Informa UK Limited, trading as Taylor & Francis Group.
This is an Open Access article distributed under the terms of the Creative Commons Attribution-NonCommercial License (http://creativecommons.org/licenses/by-nc/4.0/), which permits unrestricted non-commercial use, distribution, and reproduction in any medium, provided the original work is properly cited. The terms on which this article has been published allow the posting of the Accepted Manuscript in a repository by the author(s) or with their consent.

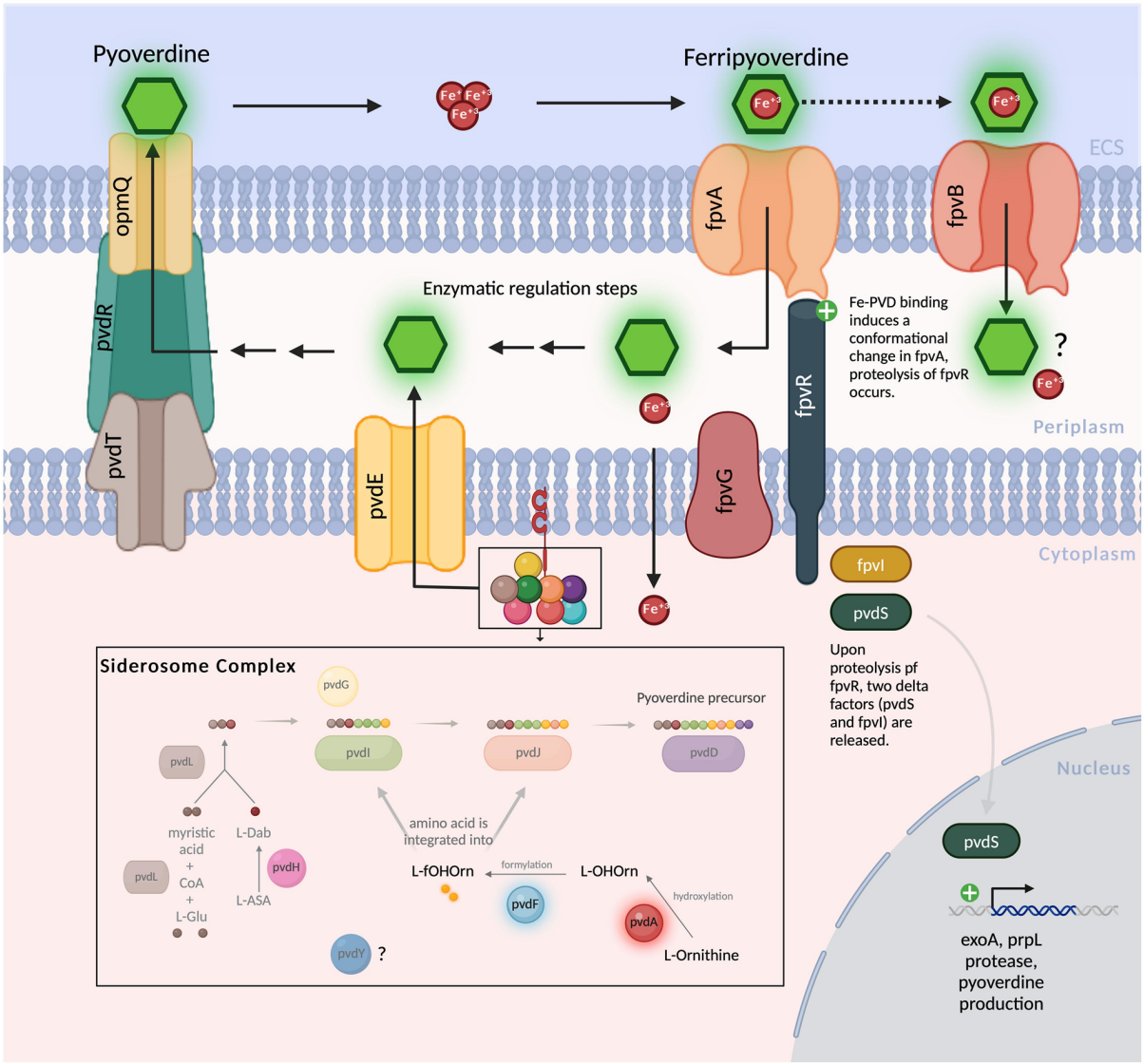


Figure 1. Pyoverdine (PVD) biosynthesis, export, uptake, and regulation in Pseudomonas aeruginosa. The precursor form of pyoverdine is assembled in the cytoplasm through the coordinated action of a multienzyme system. This complex, known as the siderosome complex, consists of nonribosomal peptide synthetases (NRPSs), including PvdL, PvdI, PvdJ, PvdD, and PvdG, together with the cytoplasmic enzymes PvdA, PvdF, and PvdH. The pyoverdine precursor is transported to the periplasm by PvdE, and the modified pyoverdine is subsequently secreted into the extracellular space through the PvdRT–OpmQ efflux pump. Upon binding ferric iron, pyoverdine forms ferripyoverdine, which is taken up through the primary receptor FpvA. Binding of ferripyoverdine to FpvA induces a conformational change and initiates a signal transduction cascade, resulting in the release of the sigma factors FpvI and PvdS from FpvR. FpvI promotes transcription of fpvA, which encodes the outer membrane transporter, whereas PvdS activates the transcription of other pyoverdine pathway genes, including exoA, prpL, and genes involved in pyoverdine biosynthesis. PvdY is a less well-characterized component of the biosynthetic machinery that is essential for the production of type II pyoverdines. Created with BioRender.com. Vatansever, C. (2026). https://BioRender.com/qcfo5jo.

biosynthesis genes show variation, *pvdL* remains highly conserved [12,14]. PvdF converts L-hydroxyornithine to L-formyl-Nδ-hydroxyornithine, which is produced by PvdA [7,12,15]. Alterations in PvdA's FAD-binding domain can irreversibly impair pyoverdine synthesis [16,17]. The pyoverdine precursor is transported from the cytoplasm to the periplasm by PvdE and exported by the PvdRT-OpmQ system [4,13,16]. Pyoverdine synthesis and *fpvA* expression are regulated by the alternative sigma factors *pvdS* and *fpvI* genes [18]. *PvdY* gene is located close to *pvdS*, but its role in pyoverdine synthesis is not well defined yet [19]. It was discovered that *pvdYII*, a variant of *pvdY* specific to strains producing type II pyoverdine, is crucial for the biosynthesis of this pyoverdine type. PvdYII catalyses the acetylation of hydroxyornithine, a key step in forming the characteristic structure of type II pyoverdine, underscoring its indispensability in this biosynthetic pathway [19].

Despite the diversity of pyoverdine types, research has predominantly focused on PVD-I, leaving significant gaps in our understanding of PVD-II and PVD-III synthesis. Moreover, data on pyoverdine synthesis and ferri-pyoverdine receptors in extensively drug resistant (XDR) *P. aeruginosa* ST235 isolates are scarce [20–22]. Given the prevalence of the ST235 clone, an efficient iron uptake mechanism could be a key survival strategy, contributing to its persistence and virulence in challenging environments. Furthermore, since pyoverdine systems are promising targets for anti-virulence therapies [21–23], understanding the unique features of the pyoverdine system in ST235 is essential for predicting potential resistance to such therapies. This study aims to investigate the type of pyoverdine secreted by XDR *P. aeruginosa* ST235 clone and variations in the pyoverdine synthesis pathway.

Methods

Clinical specimen

Clinical isolates were collected from patients hospitalized at Koşuyolu Training and Research Hospital, Istanbul and Başkent University Ankara Hospital in Türkiye between 2018 and 2020. No patient-identifying information was used in this study. A total of 27 extensively drug-resistant (XDR) *Pseudomonas aeruginosa* isolates, obtained from 27 patients with invasive infection or colonization, were included in the analysis. Antimicrobial susceptibility testing was initially performed in a routine microbiology laboratory using the VITEK® 2 system (bioMérieux, France), and resistance to colistin was confirmed by broth microdilution in accordance with EUCAST recommendations. XDR is defined as non-susceptibility to at least one agent in all but susceptibility to two or fewer antimicrobial categories [24] (Table S1). The study was conducted in accordance with the principles of the Declaration of Helsinki and was approved by the Koç University Institutional Review Board (approval no. 2018.046.IRB2.009). Written informed consent was obtained from all participants enrolled in the study.

Genomic and transcriptomic studies

The genomic DNA extraction was performed using the DNeasy UltraClean Microbial kit (QIAGEN, Germany, Catalogue #12224–250) based on the manufacturer's instructions from overnight cultures in Tryptic soy agar (Becton, Dickinson and Company, USA). Libraries were prepared using the Nextera XT DNA Library Prep Kit (Illumina, USA, Catalogue #FC-131-1002). The pooled library was sequenced on a Novaseq (Illumina, USA) platform, resulting in 150-bp paired-end reads and 50X coverage [25]. Total RNA was isolated from mid-logarithmic growth phase cultures using the QIAGEN RNeasy Kit (QIAGEN, USA, Catalogue #74106). The RNA Integrity Number (RIN) was controlled using the Agilent RNA 6000 Nano Kit (Catalogue #5067-1511). The removal of the rRNA and 5S, 16S, and 23S sequences was done by QIAseq® FastSelect™ −5S/16S/23S (Catalogue #335927) kit. After fragmentation, RNA was cleaned up using magnetic beads. The libraries were prepared with QIAseq® Stranded RNA Library Kit (Catalogue #180452) and were read in the Illumina NovaSeq platform resulting in 150-bp paired-end reads with 10 million reads per sample [26].

Gene expressions were studied by qRT-PCR to confirm transcriptomic results using primers for pyoverdine region-related genes [27]. The *rpsL* gene was used as a housekeeping gene for normalization. *P. aeruginosa* PAO1 and *P. aeruginosa* ATCC 27,853 was included as reference strains producing type I and type II pyoverdines, respectively. PAO1 is a widely used laboratory reference strain originally isolated from a wound infection, whereas ATCC 27,853 is a clinical reference strain originally isolated from a blood culture. These strains were used for normalization and comparative analyses of pyoverdine-related gene expression [28,29]. The amplification was performed in QuantStudio™ 7 Flex Real-Time PCR System. Relative gene expressions were calculated using the (-) delta–delta Ct method [30]. All experiments were performed on duplicates with three biological replicates. Statistical analysis was performed with the Mann-Whitney U test using GraphPad Prism Software v.10.0 (California, US). Error bars represented a standard deviation of the data set relative to the mean.

Bioinformatics analysis

Allelic profiles and whole-genome sequence types (wgSTs) were determined using Applied Math Bionumerics v8.1 software created by BioMerieux (Applied Math NV, Belgium), with default parameters using a scheme containing 15,136 loci and the 7 public MLST loci. Total chromosomal genes were selected, and the main relevant mutations known to be involved in iron uptake systems were investigated.

Raw sequencing data were checked for quality with FastC (v0.11.9; https://www.bioinformatics.babraham.ac.uk/projects/fastqc/). Raw reads were trimmed with Trimmomatic (v0.39) [31] for adapter sequences and low-quality bases and mapped to the reference (*P. aeruginosa* PAO1 genome, NCBI Reference

Sequence: NC_002516.2) using bwa mem from BWA (v0.7.17) [32]. For the WGS data, duplicated reads were first removed by Sambamba (v0.7.1) [30] were called using mpileup from bcftools (v1.13) and SAM/BAM handling was done with SAMtools (v1.13) [33]. Variants were annotated using SnpEff (v5.0e) [34]. For the transcriptome data, TPM (transcripts per million) values for gene expression were extracted with Rsubread (v2.14.2) [35]. Heat maps reported in this study show log2(TPM +1) expression levels of the genes. *De novo* assembly was performed with SPAdes (v3.15.4) [36] with the –isolate parameter. TPM values for scaffold-11 were corrected using the scaffold length rather than the assembly length. An automatic annotation on the *de novo* assembled scaffolds was done with Prodigal (v2.6.3) [37]. For sequence comparisons web-tool and/or stand-alone BLAST+ (v2.11.0+) was used [38]. For multiple sequence alignments, Clustal Omega web tool was used (https://www.ebi.ac.uk/jdispatcher/msa/clustalo). Protein structure comparisons were carried out on the AlphaFold Protein Structure Database (https://alphafold.ebi.ac.uk/). Functional domains were predicted using InterProScan (https://www.ebi.ac.uk/interpro/).

In uniform manifold approximation and projection (UMAP) analysis, mutation profiles of virulence genes (*Pseudomonas* species virulence factors from the Virulence Factor Database, VFDB), and Victors Virulence Factors (PHIDIAS) were used to cluster samples in two dimensions. Jaccard distance function was used to calculate distances between binary mutation profiles. R package UMAP v0.2.10.0 was used to obtain the projected coordinates.

To assess whether the structural variations observed in the pyoverdine biosynthetic locus of ST235 were conserved across the lineage, additional *P. aeruginosa* genomes were retrieved from the Bacterial and Viral Bioinformatics Resource Center (BV-BRC; https://www.bv-brc.org/). Publicly available genomes were selected based on completeness and assembly quality. A total of 130 genomes (of which 81 were ST235 and 116 were type II pyoverdine producers) representing diverse geographic locations were included in the analysis. Pyoverdine biosynthetic loci were extracted and compared with those of the reference type II pyoverdine producer ATCC 27,853 using sequence alignment and gene synteny analysis.

Colinearity between the genomes of PAO1 and ATCC27853 (NCBI Reference Sequence: NZ_KN 050641.1) was visualized with mummerplot from mummer (v4.0.0) [39] following an alignment with mummer from the same tool. Pseudomonas Genome Database (www.pseudomonas.com) was utilized for various queries, including locus tags and gene ontology information. All other custom data handling and visualization were performed using R & Python programming languages.

Structural comparison by NMR spectroscopy

Measuring pyoverdine content

Pyoverdine production of each isolate was measured according to modified methods [21,22]. Briefly, overnight cultures of *P. aeruginosa* were transferred into LB medium for growth at 37°C for 16 h with agitation. The culture was diluted 1000-fold and inoculated into modified low-iron medium (LIM: 1% 5× M9 salts (Becton Dickinson and Company Difco, USA), 1.3% Casamino Acids (Becton, Dickinson and Company Difco, USA), 1 mM $CaCl_2$, and 1 mM $MgSO_4$]) and Eagle's Minimum Essential Medium (EMEM, low iron medium, ATCC 30-2003^{TM}) in 6-well plates previously described [22]. After incubation at 37°C for 16 h, 100 µL of bacterial cultures were transferred to a 96-well plate. The bacterial growth was measured at OD_{600} nm. The fluorescence signal was measured (BioTek spectrophotometer, Synergy) with 405 nm excitation and 460 nm emission. Relative fluorescence unit readings (RFU) were normalized to the corresponding OD_{600} values to account for bacterial growth differences, yielding RFU/OD_{600} ratios (growth normalized) [22]. This assay specifically quantifies iron-free (apo) pyoverdine, which retains fluorescence and reflects active siderophore production under iron-limited conditions. To assess the effect of iron availability on pyoverdine fluorescence, parallel cultures were grown in LB medium supplemented with 25 µM $FeCl_3$, and fluorescence was measured under the same excitation/emission settings [21,22,27]. After adding iron, pyoverdine fluorescence was quenched due to ferric iron binding, serving as a comparative control for the apo-pyoverdine measurements obtained under low-iron conditions.

The experiment was performed in triplicate. *P. aeruginosa* PAO1 (type I pyoverdine producers), *P. aeruginosa* ATCC27853 (type II pyoverdine producers), and *P. aeruginosa* PAO1 delta-*pvdF* were used as control. Each experiment was performed in triplicate and repeated three times. Statistical analysis was performed with the Mann–Whitney U test using GraphPad Prism Software v10.0 (California, USA). Error bars represented a standard deviation of the data set relative to the mean.

Pyoverdine purification

Bacterial culture in the low iron medium was pelleted, and the supernatant was passed through 0.22 µM filter. After that, the supernatant was filtered with Amicon®

Ultra-15 Centrifugal Filter Unit 10 kDa (Merck, Catalogue #UFC901024) [23]. Then, the ultrafiltration method was done for filtrate from the previous step which was for metabolite and small molecule isolation, as described before [40]. Briefly in ultrafiltration, Amicon Ultra-15 centrifugal filters with a 3 kDa molecular weight cutoff (MWCO) were used, allowing retention of proteins and other high-molecular-weight components while permitting pyoverdine (≈1–1.5 kDa) to pass into the filtrate. Pyoverdine was thus separated from proteins and macromolecular contaminants by collecting the filtrate after centrifugation. The filtrate was subsequently purified by size-exclusion chromatography using an S30 gel filtration column to remove residual low-molecular-weight medium components. A final desalting step was performed using a dedicated desalting column to eliminate salts and remaining small molecules prior to fluorescence-based quantification. To determine the total pyoverdine levels (apo + Fe-bound forms), the cell-free supernatants were mixed with an equal volume of 1 M 8-hydroxyquinoline (8-HQ) solution (1:1, v/v) and incubated at room temperature to allow chelation of Fe^{3+} ions, as previously described [22]. Pyoverdine fluorescence signal was measured with a BioTek Synergy spectrophotometer at 405 nm excitation and 460 nm emission (RFU). The experiment was performed in triplicate. Each experiment was performed in triplicate and repeated three times. Statistical analysis was performed with the Mann–Whitney U test using GraphPad Prism Software v10.0 (California, USA). Error bars represented a standard deviation of the data set relative to the mean.

Iron titration was performed by serial addition of a 1 mM $FeCl_3{\cdot}6\,H_2O$ stock solution. At each step, 60 µL of the Fe stock was added to achieve a final Fe^{3+} concentration of 20 µM per increment. Absorbance was monitored between 210 and 600 nm and specifically at 370–420 nm to evaluate competitive iron binding between 8-hydroxyquinoline (8-HQ) and pyoverdine. 8-Hydroxyquinoline chelates ferric iron, thereby reducing the iron-dependent quenching of pyoverdine fluorescence. To assess the functional Fe(III)-binding behavior of type II pyoverdines, purified pyoverdines from *P. aeruginosa* ATCC 27,853 and ST235 were mixed with equimolar 8-HQ and titrated with incremental iron concentrations [8]. NMR sample preparation, data collection, and analysis: The lyophilized pyoverdine samples were dissolved in 550 µL of D_2O and transferred into a 5 mm NMR tube. 1D ^1H, 1D ^{13}C and 2D ^{13}C–^1H HMQC data acquisitions were carried out at Koç University Nanofabrication and Nanocharacterization Center (n^2STAR) on a Bruker Avance Neo Ascend NMR spectrometer operating at 500.13 MHz equipped with a 5 mm BBO double-resonance probe at 298 K and a SampleXpress sample changer. Topspin 4.2 (Bruker) and iconNMR were used to automate the data collection process. 1D ^1H spectrum consisted of 512 scans of 65,536 complex data points with a spectral width of 9615.4 Hz. 1D ^{13}C spectrum consisted of 8192 scans of 65,536 complex data points with a spectral width of 30,120.48 Hz. 2D ^{13}C–^1H HMQC spectra were recorded with 256 scans at 298 K with a ^1H spectral width of 10 ppm (1024 data points in t2) and a ^{13}C spectral width of 165 ppm (128 data points in t1). To determine the atomic correlations, to which the differences in NMR spectra belong, resonance assignments from the studies of Sultana et al., Demange et al., and Wasielewski et al. were used, as well as peak lists from BMRB 4169, and 15,629 [41–43]. The 2D data was processed by TOPSPIN 4.2 (Bruker), analysed using POKY [44] and visualized with Mnova (Mestre Lab).

Results

General features of isolates

Among 27 XDR *P. aeruginosa* isolates, 13 (48.1%) belonged to the high-risk clone ST235, and five ST446 (18.5%), three ST3078 (11.1%), two ST316 (7.4%), one ST357 (3.7%), two unassigned sequence types (7.4%) were identified. In two-dimensional UMAP visualization based on mutation profiles of *Pseudomonas* species virulence factors from the Virulence Factor Database (VFDB), and Victors Virulence Factors (PHIDIAS), all isolates were clustered by the sequence types. The ST235 cluster has markedly diverged from the other clones (Figure 2).

Comparison of the pyoverdine gene space of ST235 clones to reference strains

A comparison of WGS data to the reference PAO1 indicated several nucleotide variations in the pyoverdine biosynthesis genes for all isolates. However, the average read depth significantly decreased between *pvdE-fpvG* on the PAO1 reference genome for ST235 isolates, whereas this region was adequately represented by the WGS reads from non-ST235 isolates. Strikingly, no reads could be mapped to the *fpvA* gene within this region for ST235 isolates where the average depth remained zero (Fig. S1). To have a deeper look, a *de novo* assembly was generated for the ST235 isolate, which had sufficient WGS data (~300× average depth of coverage for the PAO1 reference genome).

The *de novo* assembly of the ST235 clone was composed of 720 scaffolds with an N50 of 229.8 kB. Scaffold-11 (~228kB), which contained the pyoverdine biosynthesis genes, did have a break in colinearity with

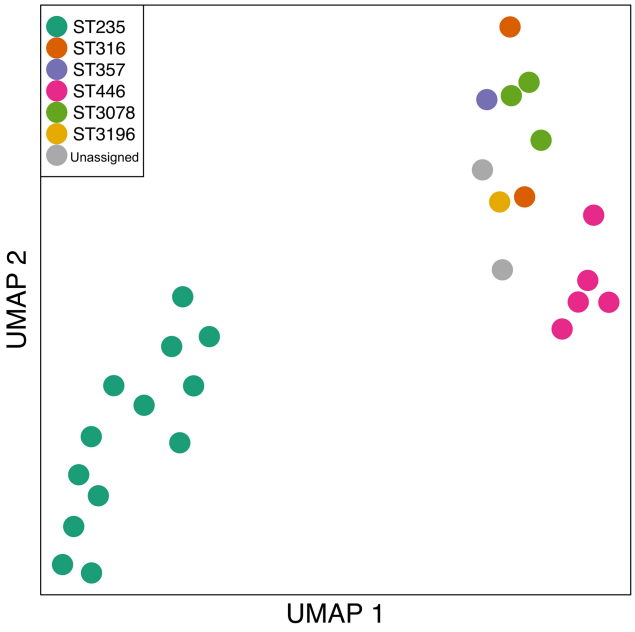


Figure 2. UMAP analysis of isolates based on the mutation profiles of Pseudomonas species virulence factors obtained from the Virulence Factor Database (VFDB) and Victors virulence factors obtained from PHIDIAS. Each isolate is shown in the UMAP plot using the color assigned to its respective sequence type. The number of points for each sequence type represents the number of isolates belonging to that sequence type.

the PAO1 genome, corresponding to the *pvdE–fpvG* region. This region was, however, colinear with *P. aeruginosa* ATCC27853 line, which carried a type II FpvA (FpvAII) and the subgroup FpvAIIb (Fig. S2). This indicated that ST235 isolates had rearranged pyoverdine loci relative to PAO1 and carried type II FpvA (FpvAII) and the subgroup FpvAIIb pyoverdine receptor.

An automated annotation of the scaffold-11 was carried out to identify potential ORFs within this scaffold. A comparison of the predicted ORFs was in close agreement with the gene organization of *P. aeruginosa* ATCC27853 and PAO1, as well, except for the region between PA2397(*pvdE*)–PA2403 (*fpvG*), consistent with our earlier observations. Even though PAO1 and ATCC27853 maintained an overall synteny across the pyoverdine biosynthesis loci, this group of genes appeared to be located in different regions of the genome. These genes were located at ~2.63MB of the 6.26 MB genome in one orientation in PAO1, and at 6.52 MB of 6.82 MB in ATCC27853 genome in the opposite orientation (Figure 3). For the ST235 isolate, this region similarly spanned 88.3 kb on scaffold-11, on a yet-unknown location in the genome.

Within the pyoverdine loci, structural differences were observed between PAO1 and ST235/ATCC27853 for *fpvA* and *pvdY* genes, as well as a major rearrangement involving the gene space containing *pvdD, pvdJ*, and *pvdI*, which appeared to be replaced by two alternative non-ribosomal protein synthetases in ST235 and ATCC27853.

Structural differences between two alternative pyoverdine biosynthesis loci

The ST235 isolates and ATCC27853 appeared to have a similar organization within the region responsible for pyoverdine biosynthesis, which had notable structural differences with the PAO1 reference genome. The most noticeable change in ST235/ATCC27853 was the apparent replacement of the *pvdD–pvdJ–pvdI* genes by two large non-ribosomal protein synthetases (NRPSs) and a probable alpha/beta hydrolase (99% identity to UniProt entry A0A5R1BDH2) that was adjacent to FpvAII (Figure 3). One of these NRPSs was 4135 aa in ST235 and almost identical to ATCC27853 homologue (99% similarity, 4127/4135 positive matches). An InterProScan search for functional domains indicated that this NRPS contains five condensation domains interspersed with 3 AMP-dependent synthetase/ligase domains. Similarly, the second NRPS was 4991 aa long in ST235, almost identical to its ATCC27853 homolog (99% similarity, 4959/4991 positive matches) and contained five condensation domains together with four AMP-dependent synthetase/ligase domains. The major receptor for ferric pyoverdine in ST235 isolates was almost identical to the FpvAII in ATCC27853, which recognized exclusively type II pyoverdines. FpvA from PAO1, only shared limited amino acid similarity with FpvAII's in ST235/ATCC27853 (44%). Consistently, *pvdY* genes in ST235 and ATCC27853 were almost identical to the *pvdYII* gene reported from strains that make type II pyoverdine [19] (Figure 3). Another PAO1 gene, PA2423 had a protein product much larger (266aa) than the protein products of its homologs in ST235/ATCC27853 (170aa). This shorter protein product, annotated as Bro-N domain containing protein in ATCC27853, had a near-perfect, C-terminal alignment to the PA2423 in PAO1.

The ST235 clone had two more structural changes on the pyoverdine loci which were not observed in ATCC27853 or PAO1. Sigma factor PvdS, which was very similar between PAO1 and ATCC27853 (187 aa for both), was also similar in the primary sequence in ST235 but was much shorter (150aa). Despite the shorter length, *pvdS* was still expressed in ST235 clones (Fig. S3), indicating that ST235 is not truncated or defective. Another ORF with 265 amino acid products was present in the ST235 isolate, adjacent to *pvdL*, but absent in either of the genomes of reference

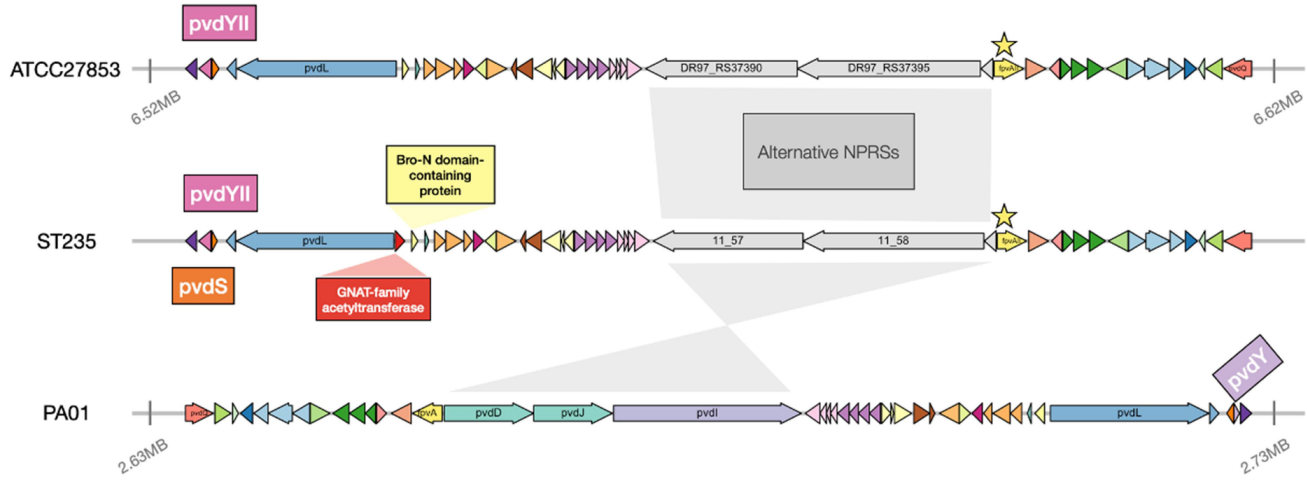


Figure 3. Comparison of pyoverdine gene content and organization among Pseudomonas aeruginosa PAO1, ATCC 27853, and the ST235 clone.

strain (Figure 3). Structural comparison of this protein to the AlphaFold Protein Structure Database suggested that the protein product of this gene is a GNAT-family N-acetyltransferase (100% identity to Uniprot entries A0A211V2D5, A0A6N0KJF6 from Pseudomonas).

Comparative analysis of publicly available *P. aeruginosa* genomes retrieved from the BV-BRC database demonstrated that the structural variations identified in the pyoverdine biosynthetic locus were conserved across the ST235 lineage. All analysed ST235 genomes (81 isolates) exhibited highly similar gene organization and sequence architecture consistent with a type II pyoverdine biosynthetic system, regardless of geographic origin. These findings indicate that ST235 represents a homogeneous lineage with respect to pyoverdine biosynthesis. In addition, other sequence types known to produce type II pyoverdine, such as ST274 and ST17, displayed a similar genomic organization of the pyoverdine locus, supporting the association between this locus architecture and type II pyoverdine production. Other prominent STs, such as ST446 and ST175, have the genomic architecture of type I pyoverdine biosynthesis. ST111, an ST that is close to ST235, has a distinct type different from both type I and type II machinery (Fig. S4)

Variations on other key components of the pyoverdine biosynthesis machinery in type II pyoverdine producers

Subtle but intriguing variations in sequences and expression profiles were also observed on other critical pyoverdine biosynthesis genes *pvdA* and *pvdF* in type II pyoverdine producers ST235/ATCC27853 compared to type I pyoverdine producer PAO1. In almost all cases, ST235 and ATCC27853 shared the same variant in reference to PAO1.

PvdA gene was enriched in non-synonymous nucleotide variants in ST235 clones (Figure 4(A) and Table S2). The *pvdA* mRNA expression was slightly lower in ST235 but not statistically significant with a TPM mean of 77.98 compared to the mean of 117.2 non-ST235 ($p = 0.132$) (Figure 4(B)). The RT-PCR confirmed the transcriptomic data with a mean fold change of −13.46 in ST235 vs −0.41 in other clones ($p < 0.0001$).

In *pvdA*, non-synonymous nucleotide variants accumulated between nucleotides 46 and 1192. The 803 G > A mutation was found in the protein–protein interaction area of the A and B chains (amino acids 242–337), while the Pro168Ala mutation was detected in the FAD binding site (Figures. 4(A,C,D)). Non-synonymous nucleotide variants in the active site of *pvdA* (46 G > A, … 1192A > T, Table S2) were consistent across all ST235 group isolates (Figure 4(A)). Among these, Gln121Ala (363 G > C), Arg132Ser (395 G > C), Arg268Gln (803 G > A), His270Gly (809A > G), and Ser398Cys (1192A > T) may alter the structural configuration or enzymatic function of the emergent enzyme form (Figures. 4(D,E) and Table S2).

The *pvdF* gene, another crucial component of the siderosome, exhibited enrichment in non-synonymous nucleotide variants in ST235 clones (Figure 5(A) and Table S2). Notably, *pvdF* mRNA expression was significantly lower in ST235 clones (mean TPM 26.71) compared to non-ST235 clones (mean TPM 73.8, $p = 0.0015$) (Figure 5(B)). Non-synonymous nucleotide variants accumulated in the active site of PvdF, including Ala64Pro (190 G > C), Ser125Arg (373A > C), Glu176Ala (528 G > C), Tyr186Trp (557A > G), Tyr193His (577T > C), Val200Ile (598 G > A), Glu241Lys (721 G > A), and Asn258Asp (772A > G) (Figures. 5(A,C)). Many of these

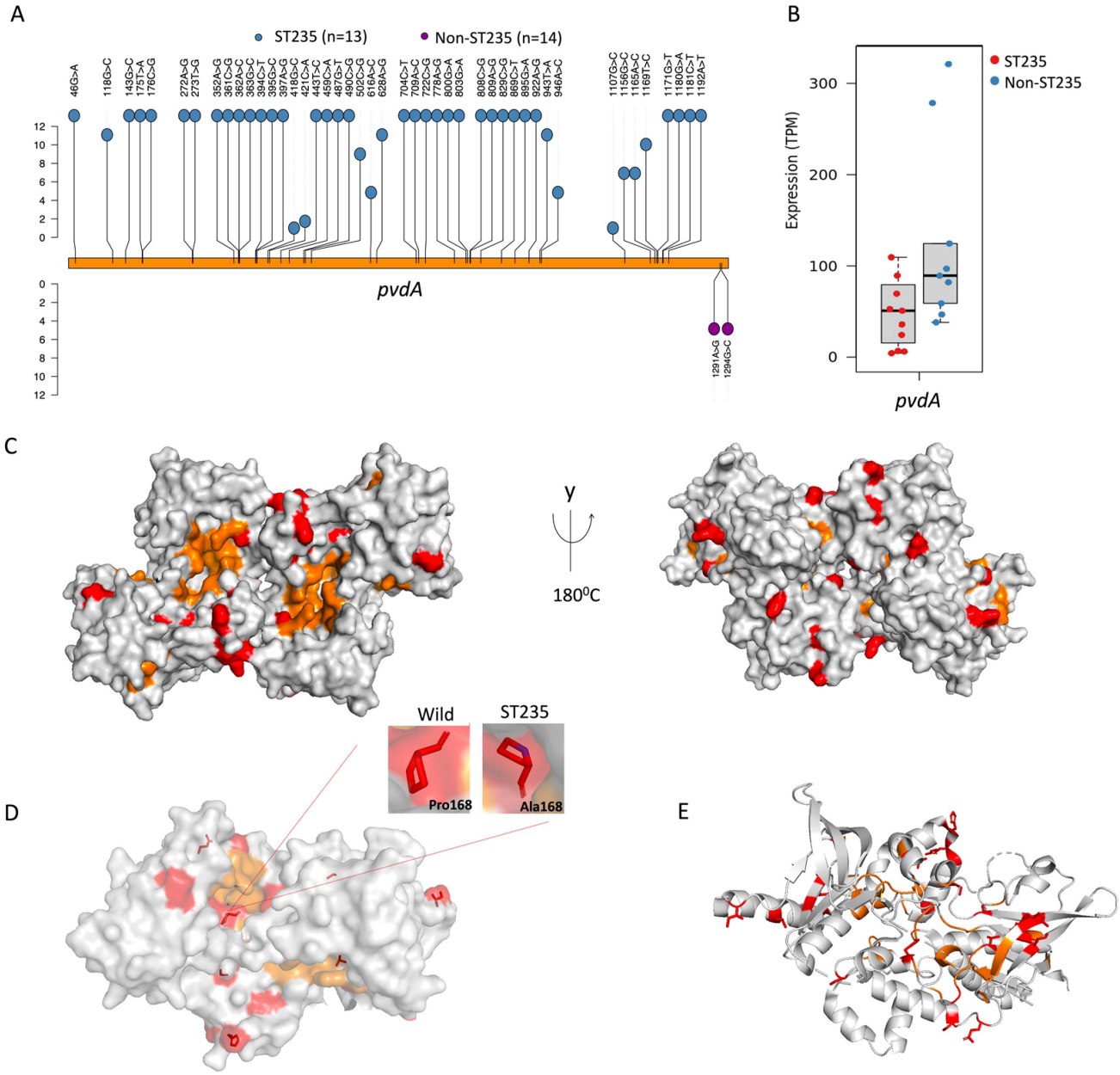


Figure 4. PvdA. A. Lollipop plots showing variant distribution in *pvdA* sequences. Lollipop height is proportional to the number of isolates that had non-synonymous nucleotide variants. The non-synonymous nucleotide variants were shown on the top of each lollipop. The non-synonymous variants were shown as a blue dot in the ST235 (n = 13) and a purple dot in the non-ST235 (n = 14). B. Transcript per million (TPM) expression levels between ST235 and non-ST235 in the *pvdA* gene. Error bars represent the standard deviation of a data set. C. Structure of PvdA (PDB code: 3S5W). To the left, the entire protein structure is shown as a surface model, with red labeled variants and orange labeled ligands binding areas. To the right, the protein is rotated 180 degrees on the y-axis. D. Structure of PvdA (one chain) is shown as a surface model, with a transparent and gray-tinted surface, and mutations are colored in red. On the top, closer view of mutations (Pro168Ala). E. Structure of PvdA (one chain) is shown as a ribbon. Images generated with The PyMOL Molecular Graphics System, Version 3.1.8, Schrödinger, LLC with data files obtained through the Protein Data Bank.

variants could potentially affect the secondary structure of the protein, with the Ala64Pro (190 G > C) mutation being particularly noteworthy due to its proximity to the enzymatic core (Figures. 5(D,E)).

In addition to pyoverdine-associated genes, we evaluated the transcript levels of alternative iron acquisition systems, including pyochelin biosynthesis/transport and heme uptake pathways. Also, *prpL* and toxA, which are regulated by *pvdS*. Expression levels of key heme uptake genes, *hasP* (PA3407), *hasR* (PA3408), *phuT* (PA4708), and *phuR* (PA4710), were comparable between ST235 and non-ST235 isolates, with no statistically significant differences (p = 0.98, 0.45, 0.97, and 0.56, respectively; Fig. S5A). Similarly, genes involved in pyochelin biosynthesis

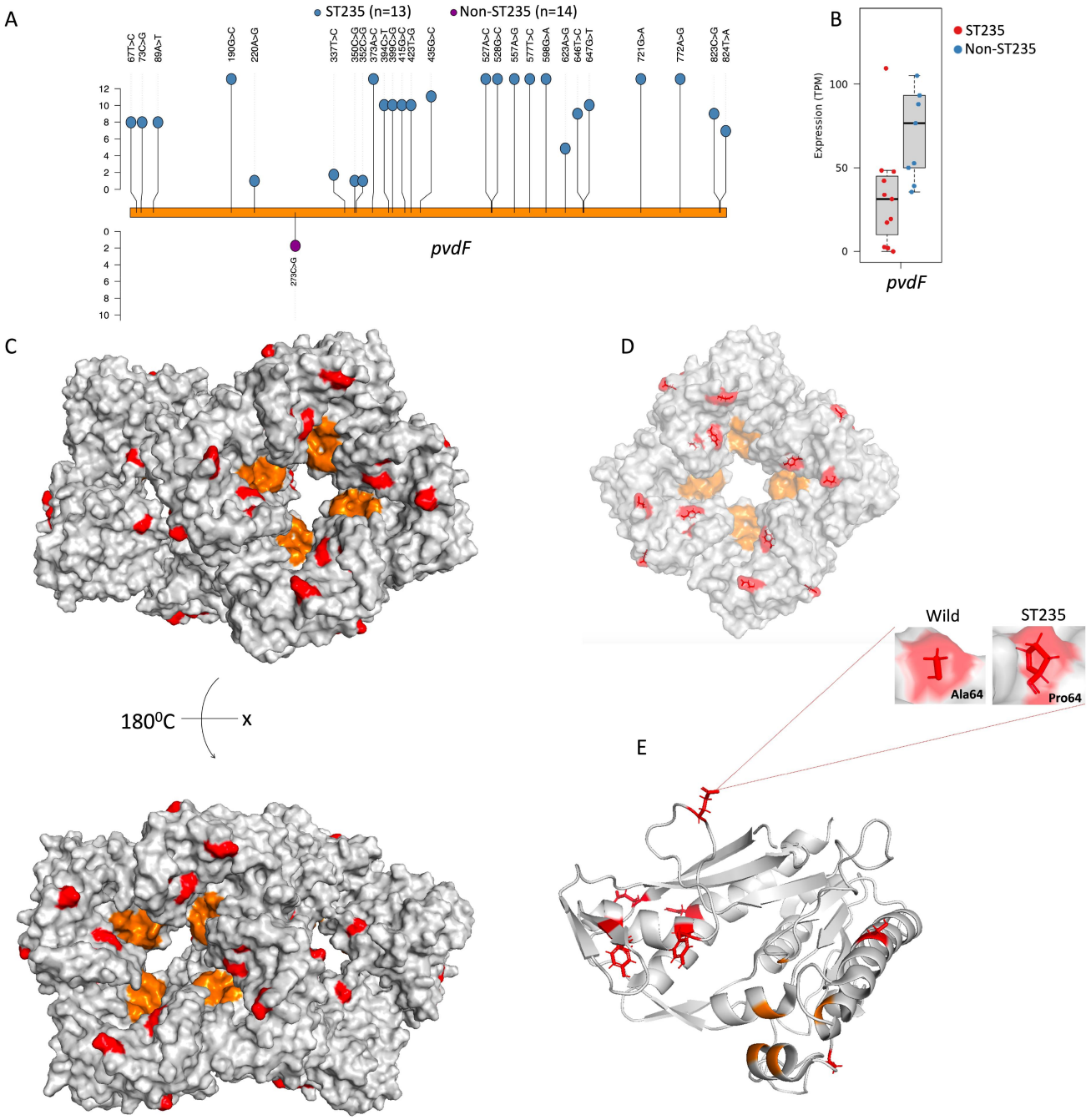


Figure 5. PvdF. A. Lollipop plots showing variant distribution in *pvdF* sequences. Lollipop height is proportional to the number of isolates that had non-synonymous nucleotide variants. The non-synonymous nucleotide variants were shown on the top of each lollipop. The non-synonymous nucleotide variants were shown as a blue dot in the ST235 ($n = 13$) and a purple dot in the non-ST235 ($n = 14$). B. Transcript per million (TPM) expression levels between ST235 and non-ST235 in the *pvdF* gene. Error bars represent the standard deviation of a data set. C. Structure of PvdF (PDB code: 6CUL). To the left, the entire protein structure is shown as a surface model, with red labeled variants and orange-labeled ligands binding areas. To the right, the protein is rotated 180 degrees on the y-axis. D. Structure of PvdF (one chain) is shown as a surface model, with a transparent and gray-tinted surface, and mutations are colored in red. On the top, closer view of mutations (Ala64Pro). E. Structure of PvdF (one chain) is shown as a ribbon. Images generated with The PyMOL Molecular Graphics System, Version 3.1.8, Schrödinger, LLC with data files obtained through the Protein Data Bank.

(*pchF* (PA4225), *pchE* (PA4226), *pchC* (PA4229), and *pchA* (PA4231)) showed slightly higher expression levels in ST235 isolates; however, these differences were not statistically significant ($p = 0.88$, 0.75, 0.87, and 0.46, respectively; Fig. S5B). All isolates carried both *prpL* and *toxA*. While *toxA* expression was higher in ST235 isolates

compared to non-ST235 isolates (mean TPM: 59.3 vs 39.8) (Figure 6(A)), this difference did not reach a statistical significance ($p = 0.10$). In contrast, *prpL* expression levels were similar between the two groups (mean TPM: 101.3 vs 97.3; $p = 0.97$) (Fig. S6B).

Extracellular pyoverdine levels and structural analysis of pyoverdine

There was no significant difference in apo-pyoverdine fluorescence signals between ST235 and non-ST235 *P. aeruginosa*, with mean relative fluorescence units per OD_{600} (RFU/OD_{600}) of 59.996 and 74.112 ($p = 0.988$) in LIM and 80.412 and 72.164 ($p = 0.889$) in EMEM, respectively. Signals were measured in two different low iron mediums, EMEM and LIM (Figure 6(A)). Pyoverdine fluorescence signals were also depleted with the addition of $FeCl_3$ to confirm production (Fig. S7). The total pyoverdine (apo + Fe-bound forms) concentration produced by ST235 was higher than non-ST235 (22.668 vs 15.835 RFU, $p < 0.001$) (Figure 6(B)).

NMR analysis of pyoverdine from *P. aeruginosa* strains revealed structural differences in ST235 compared to non-ST235 strains. The 2D H-C HMQC spectra showed no differences between pyoverdine from PAO1 and non-ST235 strains (Fig. S8). However, two key differences were identified in pyoverdine from the ST235 strain compared to PAO1 (Figure 6(C)). The first was the absence of a peak in the region of 3.40 ppm (H)-45.80 ppm (C) in the HMQC spectrum of pyoverdine derived from the ST235 strain; the second was the shift of the chemical displacement values of the peak located in the region of 8.06 ppm (H)-135.42 ppm (C) to the region of 8.12 ppm (H)-135.24 ppm (C). The C–H bond corresponding to the chemical shift values of 3.40 ppm (H)-45.80 ppm (C) was in the OHOrn7 (delta protons) region of pyoverdine. The C-H bond corresponding to the chemical shift values of 8.06 ppm (H)-135.42 ppm (C) was in the chromophore region (Chr C9) of the pyoverdine molecule (Figure 6(C)).

In the competitive iron titration assays with *P. aeruginosa* ATCC 27,853 and ST235 isolates, the absorbance progressively decreased with increasing iron concentration, consistent with ferripyoverdine formation, and reached a plateau at ~140 µM Fe(III) (Fig. S9). No further changes were observed beyond this point. This result confirmed that *P. aeruginosa* ATCC 27,853 and ST235 pyoverdines have a similar saturation profile (Fig. S9).

Discussion

Pyoverdine loci are one of the most diverse regions in the *P. aeruginosa* genome and play a crucial role in activating virulence mechanisms [5,45]. In iron competition, modifications in the pyoverdine system could offer a selective advantage to *P. aeruginosa*, facilitating its successful spread. Despite the high energy cost of pyoverdine production, the ST235 clone has managed to retain both high virulence capacity and extensive antibiotic resistance capacity. Here, we presented a modified type II pyoverdine system in the *P. aeruginosa* ST235 high-risk clone.

In *P. aeruginosa*, ferric pyoverdine receptors are specific to the type of pyoverdine they transport [5]. We identified through *de novo* WGS analysis that all ST235 isolates possessed a type II pyoverdine system, characterized by the ferri pyoverdine receptor II (FpvAII), specifically, the FpvAIIb subgroup. This type II system was further confirmed by the presence of the acetyltransferase *pvdYII* [19] distinguishing from non-ST235 isolates, which exhibited a type I pyoverdine system with FpvAI. PvdYII is essential for type II pyoverdine biosynthesis [19] and ST235 displayed unique modification within this established system. Notably, PvdYII (337aa) of ST235, was longer than the PvdY of PAO1 strain (155aa) and highly divergent in sequence, showing only short stretches of aligning sequences. The ferri-pyoverdine receptors permit the entry of different pyoverdine and also bacteriocins (pyocin) [6]. Type II FpvA the receptor has the highest specificity and does not permit the entrance of other types of pyoverdine. This specificity may support the survival of the ST235 strains in the presence of bacteriocins in the gut or in the environment [46].

The co-evolution of pyoverdine loci with their ferri-pyoverdine receptors ensures a mutual specificity between the pyoverdine type and the receptor [5]. To date, the majority of studies have reported in the biosynthesis of type I pyoverdine, but the genome of pyoverdine type II biosynthesis has not been well explored [9,45]. This study presents significant genomic rearrangements in the type II pyoverdine biosynthesis genes. We observed the replacement of the *pvdD–pvdJ–pvdI* gene cluster with two large non-ribosomal peptide synthetases (NRPSs) and an alpha/beta hydrolase. This reorganization aligns with previous observations by Smith et al. (2005) on the diversity of pyoverdine loci among *P. aeruginosa* strains [45]. The presence of these large NRPSs (4135aa and 4991 aa) with multiple condensation and AMP-dependent synthetase/ligase domains suggests a distinct biosynthetic pathway for type II pyoverdines. This finding was consistent with the modular nature and evolutionary plasticity of NRPSs in siderophore biosynthesis [47]. The high similarity between ST235 and ATCC27853 NRPSs

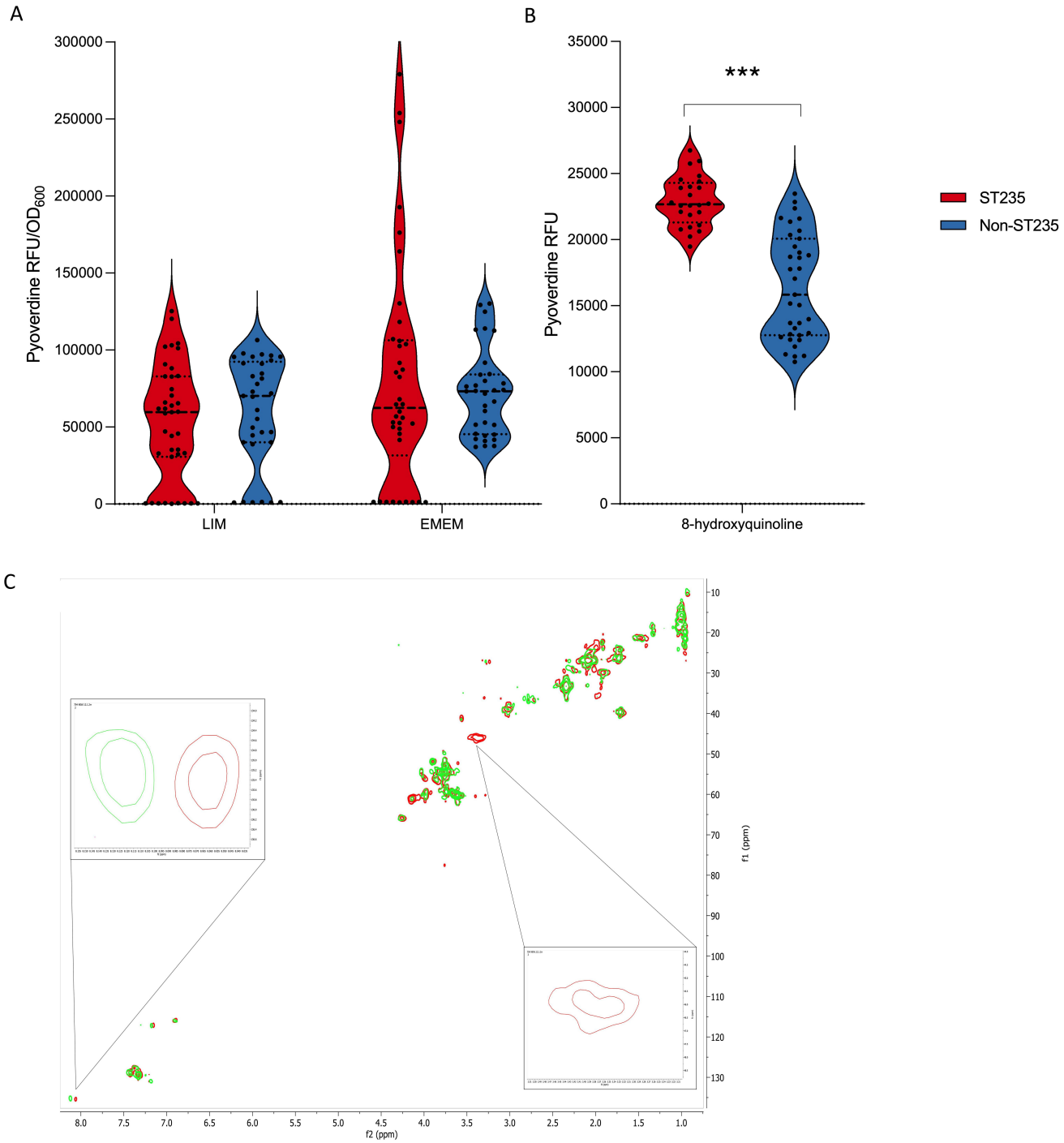


Figure 6. (A) Extracellular (apo) pyoverdine production by ST235 and non-ST235 isolates grown in LIM and EMEM. No significant difference in pyoverdine levels was observed between ST235 and other clones (mean RFU/OD_{600}: 59.996 vs 74.112; $p = 0.988$). (B) Total pyoverdine production (apo + Fe-bound forms) in ST235 and non-ST235 isolates following 8-hydroxyquinoline treatment. ST235 isolates exhibited significantly higher total pyoverdine levels compared with non-ST235 isolates (22.668 vs 15.835 RFU;$p < 0.001$). Violin plots show the distribution of measurements, with overlaid dots representing individual measurements from technical replicates. Each isolate represents a biological replicate, and sample sizes are indicated in the figure. C. Comparison of the 2D $^{1}H–^{13}C$ HMQC spectra of the pyoverdine derived from PAO1 (red) and ST235 (green) strains and distinctive differences were identified on the spectrum when comparing pyoverdine from the ST235 strain to pyoverdine from the PAO1.

(99% similarity) indicates a conserved biosynthetic mechanism among type II pyoverdine producers. We postulate that the proximity of alpha/beta hydrolase gene to FpvAII may lead to the concomitant evolution of type II pyoverdine and its receptor. These genomic adaptations likely reflect the evolutionary pressure on *P. aeruginosa* to diversify its iron acquisition strategies [8].

The genomic and structural modifications were identified in the biosynthesis pathway *of P. aeruginosa* ST235 clone. The key finding was the truncated *pvdS* gene in ST235, encoding a shorter sigma factor (150 aa vs 187 aa in PAO1) that lacks one Sigma70_r2 domain. This truncated PvdS could impact the regulation of pyoverdine biosynthesis genes, potentially altering iron acquisition and virulence [46]. In line with the regulatory role of *pvdS*, although *toxA* expression was higher in ST235 isolates, and *prpL* levels were comparable between groups, these differences were not statistically significant, suggesting that *pvdS* truncation may not uniformly translate into downstream transcriptional changes. Additionally, ST235 possesses a novel open reading frame (ORF) adjacent to *pvdL*, encoding a 265-amino-acid GNAT-family N-acetyltransferase. GNAT enzymes play diverse roles in bacterial physiology, including antibiotic resistance, metabolic regulation, and iron homeostasis [48]. Song et al. (2022) demonstrated that GNAT toxins can regulate iron-uptake-related genes, contributing to bacterial virulence [49]. The presence of this GNAT-family enzyme in ST235 probably enhances the iron acquisition efficiency of this clone.

Numerous non-synonymous variations in the *pvdA* and *pvdF* genes of ST235 were identified in this study. As these genes are important for pyoverdine biosynthesis [17], variations in pyoverdine precursor synthesis genes could lead to changes in the pyoverdine molecule structure [12]. In all ST235 isolates, we detected the Pro168Ala mutation in the FAD-binding site of PvdA along with many non-synonymous mutations. There were significant amino acid side-chain changes in the PvdA enzyme, potentially causing structural and functional alterations in the protein. Studies have also indicated that a single amino acid substitution in the FAD-binding site of PvdA could terminate pyoverdine biosynthesis [17].

Despite such structural modifications within the pyoverdine biosynthetic locus, we detected higher pyoverdine production in ST235 than non-ST235 isolates (Figure 6). Besides, the titration results confirmed the extraordinarily strong Fe(III) chelator activity of pyoverdine from ST235, consistent with previously reported binding affinities (Fig. S9) [4,8]. In addition, alternative iron acquisition pathways, including pyochelin biosynthesis and heme uptake systems, did not show significant transcriptional differences between ST235 and non-ST235 isolates. These results demonstrate that the multidrug-resistant ST235 clone maintains pyoverdine-mediated iron acquisition at levels equivalent to the reference type II producer. NMR analysis revealed distinctive chemical shifts in the pyoverdine molecules secreted by ST235 isolates, particularly in the OHOrn7 (delta protons) region, which were absent in non-ST235 and PAO1 strains (Fig. 6(C) and S8). This shift could be due to the increased interaction of the chromophore region with iron or structural changes in the ornithine region of pyoverdine, potentially causing steric effects on nearby atoms [9]. This observation suggests that the ST235 clone may possess compensatory mechanisms that maintain pyoverdine production despite these potentially disruptive mutations. Understanding these pathways could reveal how the ST235 clone adapts to maintain essential functions despite genetic changes.

In this context, non-redox-active iron mimetics such as gallium (Ga^{3+}), which enter bacterial iron uptake pathways including pyoverdine-mediated systems without supporting redox activity, have emerged as promising anti-*Pseudomonas* agents [50]. Given the structural and functional features of the type II pyoverdine system in ST235, this clone could exhibit altered susceptibility to gallium-based therapies, providing a rationale for future investigation of iron-mimetic antimicrobial strategies targeting high-risk lineages.

The PvdF converts ornithine hydroxylamine to hydroxamate, is crucial for pyoverdine production, and deletions in this gene inhibit pyoverdine synthesis [15]. We identified Val200Ile (598 G > A) amino acid alteration in the PvdF of all ST235 isolates. The amino acids between 197 and 214 in the PvdF molecule are a key region for OHOrn substrate binding and form an antiparallel β-sheet, providing additional stability to the protein [51]. Therefore, the variations in this chain are likely to change the structural configuration or enzymatic function of the PvdF. ST235 clone-specific variations in *pvdA* and *pvdF*, coupled with a significant reduction in their expression (Figure 4(B) and 5(B)), suggest considerable alterations in the pyoverdine precursor structure. These findings highlight the need for future studies to investigate the compensatory mechanisms that sustain pyoverdine production despite these mutations.

In conclusion, *P. aeruginosa* ST235 clone chelates iron with type II pyoverdine and transports it into the cell via the highly specific FpvA II receptor. The extracellular pyoverdine production remains unchanged despite genomic changes in the regulator precursor. This suggests that these modifications provide an evolutionary advantage by allowing the pyoverdine system to function more effectively without incurring additional energy costs. This study opens avenues for further research into other evolutionary advantages that contribute to multidrug resistance, potentially revealing vulnerabilities for developing antivirulence-targeted therapies. This research presents opportunities for investigating further evolutionary benefits of multidrug resistance, which could help to identify limitations for developing antivirulence-targeted therapies.

Acknowledgements

We acknowledge Koç University Nanofabrication and Nanocharacterization Center (n^2STAR) for access to the infrastructure. We also acknowledge Prof. Isabelle J Schalk, University of Strasbourg, for providing *P. aeruginosa* PAO1 delta-*pvdF*. This manuscript was produced from Cansel Vatansever's PhD thesis, numbered 753706.

Author contributions

CRediT: **Cansel Vatansever:** Conceptualization, Data curation, Formal analysis, Funding acquisition, Investigation, Methodology, Project administration, Resources, Software, Supervision, Validation, Visualization, Writing – original draft, Writing – review & editing; **Ani Akpınar:** Conceptualization, Data curation, Formal analysis, Investigation, Methodology, Software, Validation, Visualization, Writing – original draft; **Selin Kolsuz:** Data curation, Investigation, Methodology, Visualization, Writing – original draft; **Gulin Özcan:** Investigation, Methodology; **Güz Ekinci:** Data curation, Investigation, Methodology, Visualization; **Özlem Azap:** Conceptualization, Methodology, Resources; **Alp Eren Kazar:** Data curation, Investigation, Methodology, Writing – original draft; **Kerem Kahraman:** Data curation, Investigation, Methodology; **Emir Ural:** Investigation, Methodology; **Çağdaş Dağ:** Conceptualization, Data curation, Formal analysis, Investigation, Methodology, Validation, Visualization, Writing – original draft; **Mehmet Gönen:** Conceptualization, Data curation, Formal analysis, Investigation, Methodology; **Fusun Can:** Conceptualization, Data curation, Formal analysis, Funding acquisition, Investigation, Methodology, Project administration, Supervision, Validation, Writing – original draft.

Funding

This work was funded by The Scientific and Technological Research Council of Turkey [TUBITAK], [Project no. 119S446 and 122S343] and Koç University-İş Bank Center for Infectious Diseases (KUISCID).

Disclosure statement

No potential conflict of interest was reported by the author(s).

ORCID

Cansel Vatansever http://orcid.org/0000-0003-3703-1882
Ani Akpınar http://orcid.org/0000-0001-6863-7436
Selin Kolsuz http://orcid.org/0000-0002-9067-9939
Gulin Özcan http://orcid.org/0000-0003-3364-514X
Güz Ekinci http://orcid.org/0000-0002-9512-836X
Özlem Azap http://orcid.org/0000-0002-3171-8926
Alp Eren Kazar http://orcid.org/0009-0001-1609-748X
Çağdaş Dağ http://orcid.org/0000-0003-1595-431X
Mehmet Gönen http://orcid.org/0000-0002-2483-075X
Fusun Can http://orcid.org/0000-0001-9387-2526

Data availability statement

All supplementary figures and tables supporting the findings of this study have been deposited in the Figshare repository and are publicly available (Dataset. https://doi.org/10.6084/m9.figshare.31347037.v1) [52].

The raw data supporting the findings of this study have been deposited in the NCBI BioProject repository under the accession number PRJNA1241513 [53]

References

[1] Del Barrio-Tofino E, Lopez-Causape C, Oliver A. *Pseudomonas aeruginosa* epidemic high-risk clones and their association with horizontally-acquired beta-lactamases: 2020 update. Int J Antimicrob Agents. 2020;56(6):106196.
[2] Vatansever C, Menekse S, Dogan O, et al. Co-existence of OXA-48 and NDM-1 in colistin resistant *Pseudomonas aeruginosa* ST235. Emerg Microbes Infect. 2020;9(1):152–154. doi: 10.1080/22221751.2020.1713025
[3] Treepong P, Kos VN, Guyeux C, et al. Global emergence of the widespread Pseudomonas aeruginosa ST235 clone. Clin Microbiol Infect. 2018;24(3):258–266. doi: 10.1016/j.cmi.2017.06.018
[4] Schalk IJ, Guillon L. Pyoverdine biosynthesis and secretion in *Pseudomonas aeruginosa*: implications for metal homeostasis. Environ Microbiol. 2013;15(6):1661–1673. doi: 10.1111/1462-2920.12013
[5] Tummler B, Cornelis P. Pyoverdine receptor: a case of positive Darwinian selection in *Pseudomonas aeruginosa*. J Bacteriol. 2005;187(10):3289–3292. doi: 10.1128/JB.187.10.3289-3292.2005
[6] Bodilis J, Ghysels B, Osayande J, et al. Distribution and evolution of ferripyoverdine receptors in *Pseudomonas aeruginosa*. Environ Microbiol. 2009;11(8):2123–2135. doi: 10.1111/j.1462-2920.2009.01932.x
[7] Ghssein G, Ezzeddine Z. A review of Pseudomonas aeruginosa metallophores: pyoverdine, pyochelin and pseudopaline. Biol (Basel). 2022;11(12):1711. doi: 10.3390/biology11121711
[8] Visca P, Imperi F, Lamont IL. Pyoverdine siderophores: from biogenesis to biosignificance. Trends Microbiol. 2007;15(1):22–30. doi: 10.1016/j.tim.2006.11.004
[9] Ringel MT, Bruser T. The biosynthesis of pyoverdines. Microb Cell. 2018;5(10):424–437. doi: 10.15698/mic2018.10.649
[10] de Chial M, Ghysels B, Beatson SA, et al. Identification of type II and type III pyoverdine receptors from *Pseudomonas aeruginosa*. Microbiol (Read). 2003;149(Pt 4):821–831. doi: 10.1099/mic.0.26136-0
[11] Ghysels B, Dieu BTM, Beatson SA, et al. Fpvb, an alternative type I ferripyoverdine receptor of *Pseudomonas aeruginosa*. Microbiol (Read). 2004;150(Pt 6):1671–1680. doi: 10.1099/mic.0.27035-0
[12] Gasser V, Guillon L, Cunrath O, et al. Cellular organization of siderophore biosynthesis in *Pseudomonas aeruginosa*: evidence for siderosomes. J Inorg Biochem. 2015;148:27–34. doi: 10.1016/j.jinorgbio.2015.01.017

[13] Schalk IJ, Perraud Q. *Pseudomonas aeruginosa* and its multiple strategies to access iron. Environ Microbiol. 2023;25(4):811–831. doi: 10.1111/1462-2920.16328
[14] Mettrick KA, Lamont IL. Different roles for anti-sigma factors in siderophore signalling pathways of *Pseudomonas aeruginosa*. Mol Microbiol. 2009;74 (5):1257–1271. doi: 10.1111/j.1365-2958.2009.06932.x
[15] Kenjic N, Hoag MR, Moraski GC, et al. Pvdf of pyoverdin biosynthesis is a structurally unique N(10)-formyltetrahydrofolate-dependent formyltransferase. Arch Biochem Biophys. 2019;664:40–50.
[16] Imperi F, Tiburzi F, Visca P. Molecular basis of pyoverdine siderophore recycling in Pseudomonas aeruginosa. Proc Natl Acad Sci USA. 2009;106-(48):20440–20445. doi: 10.1073/pnas.0908760106
[17] Imperi F, Putignani L, Tiburzi F, et al. Membrane-association determinants of the omega-amino acid monooxygenase PvdA, a pyoverdine biosynthetic enzyme from *Pseudomonas aeruginosa*. Microbiol (Read). 2008;154(Pt 9):2804–2813.
[18] Edgar RJ, Xu X, Shirley M, et al. Interactions between an anti-sigma protein and two sigma factors that regulate the pyoverdine signaling pathway in *Pseudomonas aeruginosa*. BMC Microbiol. 2014;14 (1):287. doi: 10.1186/s12866-014-0287-2
[19] Lamont IL, Martin LW, Sims T, et al. Characterization of a gene encoding an acetylase required for pyoverdine synthesis in *Pseudomonas aeruginosa*. J Bacteriol. 2006;188(8):3149–3152. doi: 10.1128/JB.188.8.3149-3152.2006
[20] Imperi F, Visca P. Subcellular localization of the pyoverdine biogenesis machinery of *Pseudomonas aeruginosa*: a membrane-associated "siderosome". FEBS Lett. 2013;587(21):3387–3391. doi: 10.1016/j.febslet.2013.08.039
[21] Kang D, Revtovich AV, Chen Q, et al. Pyoverdine-dependent virulence of Pseudomonas aeruginosa isolates from cystic fibrosis patients. Front Microbiol. 2019;10:2048. doi: 10.3389/fmicb.2019.02048
[22] Kang D, Kirienko DR, Webster P, et al. Pyoverdine, a siderophore from P*seudomonas aeruginosa*, translocates into *C. elegans*, removes iron, and activates a distinct host response. Virulence. 2018;9(1):804–817. doi: 10.1080/21505594.2018.1449508
[23] Wang X, Kleerekoper Q, Revtovich AV, et al. Identification and validation of a novel anti-virulent that binds to pyoverdine and inhibits its function. Virulence. 2020;11(1):1293–1309. doi: 10.1080/21505594.2020.1819144
[24] Magiorakos AP, Srinivasan A, Carey RB, et al. Multidrug-resistant, extensively drug-resistant and pandrug-resistant bacteria: an international expert proposal for interim standard definitions for acquired resistance. Clin Microbiol Infect. 2012;18(3):268–281. doi: 10.1111/j.1469-0691.2011.03570.x
[25] Bogaerts B, Winand R, Van Braekel J, et al. Evaluation of WGS performance for bacterial pathogen characterization with the Illumina technology optimized for time-critical situations. Microb Genom. 2021;7(11). doi: 10.1099/mgen.0.000699
[26] Aiewsakun P, Prombutara P, Siregar TAP, et al. Transcriptional response to the host cell environment of a multidrug-resistant Mycobacterium tuberculosis clonal outbreak Beijing strain reveals its pathogenic features. Sci Rep. 2021;11(1):3199. doi: 10.1038/s41598-021-82905-x
[27] Kang D. Siderophore-mediated virulence and its inhibition in *Pseudomonas aeruginosa 2023*.
[28] Stover CK, Pham XQ, Erwin AL, et al. Complete genome sequence of Pseudomonas aeruginosa PAO1, an opportunistic pathogen. Nature. 2000;406 (6799):959–964. doi: 10.1038/35023079
[29] Tappe R, Taraz K, Budzikiewicz H, et al. Structure elucidation of a pyoverdin produced by *Pseudomonas aeruginosa* ATCC 27 853. J für Praktische Chem. 1993;335(1):83–87. doi: 10.1002/prac.19933350113
[30] Livak KJ, Schmittgen TD. Analysis of relative gene expression data using real-time quantitative PCR and the 2(-delta delta C(T)) method. Methods. 2001;25 (4):402–408. doi: 10.1006/meth.2001.1262
[31] Bolger AM, Lohse M, Usadel B. Trimmomatic: a flexible trimmer for Illumina sequence data. Bioinformatics. 2014;30(15):2114–2120. doi: 10.1093/bioinformatics/btu170
[32] Li H, Durbin R. Fast and accurate short read alignment with Burrows-Wheeler transform. Bioinformatics. 2009;25(14):1754–1760. doi: 10.1093/bioinformatics/btp324
[33] Danecek P, Bonfield JK, Liddle J, et al. Twelve years of SAMtools and BCFtools. Gigascience. 2021;10(2). doi: 10.1093/gigascience/giab008
[34] Cingolani P, Platts A, Wang le L, et al. A program for annotating and predicting the effects of single nucleotide polymorphisms, SnpEff: sNPs in the genome of Drosophila melanogaster strain w1118; iso-2; iso-3. Fly (Austin). 2012;6(2):80–92. doi: 10.4161/fly.19695
[35] Liao Y, Smyth GK, Shi W. The R package rsubread is easier, faster, cheaper and better for alignment and quantification of RNA sequencing reads. Nucleic Acids Res. 2019;47(8):e47. doi: 10.1093/nar/gkz114
[36] Prjibelski A, Antipov D, Meleshko D, et al. Using SPAdes de novo assembler. Curr Protoc Bioinf. 2020;70(1):e102. doi: 10.1002/cpbi.102
[37] Hyatt D, Chen G-L, LoCascio PF, et al. Prodigal: prokaryotic gene recognition and translation initiation site identification. BMC Bioinf. 2010;11(1):119. doi: 10.1186/1471-2105-11-119
[38] Camacho C, Coulouris G, Avagyan V, et al. Blast+: architecture and applications. BMC Bioinf. 2009;10 (1):421. doi: 10.1186/1471-2105-10-421
[39] Marcais G, Delcher AL, Phillippy AM, et al. MUMmer4: a fast and versatile genome alignment system. PLoS Comput Biol. 2018;14(1):e1005944. doi: 10.1371/journal.pcbi.1005944
[40] Dağ Ç, Göçenler O, Tozkoparan CD. The analysis of metabolic content of traditional milk collected from three regions in Turkey by NMR spectroscopy. Gıda. 2022;47(5):765–775. doi: 10.15237/gida.GD22042
[41] Sultana R, Siddiqui BS, Taraz K, et al. A pyoverdine from *Pseudomonas putida* CFML 90–51 with a Lys epsilon-amino link in the peptide chain. Biometals. 2000;13(2):147–152. doi: 10.1023/A:1009212729408

[42] Demange P, Wendenbaum S, Linget C, et al. Bacterial siderophores: structure and NMR assignment of pyoverdins Pa, siderophores of *Pseudomonas aeruginosa* ATCC 15692. Biol Met. 1990;3(3–4):155–170. doi: 10.1007/BF01140574

[43] Wasielewski E, Tzou DL, Dillmann B, et al. Multiple conformations of the metal-bound pyoverdine PvdI, a siderophore of *Pseudomonas aeruginosa*: a nuclear magnetic resonance study. Biochemistry. 2008;47(11):3397–3406. doi: 10.1021/bi702214s

[44] Lee W, Rahimi M, Lee Y, et al. Poky: a software suite for multidimensional NMR and 3D structure calculation of biomolecules. Bioinformatics. 2021;37(18):3041–3042. doi: 10.1093/bioinformatics/btab180

[45] Smith EE, Sims EH, Spencer DH, et al. Evidence for diversifying selection at the pyoverdine locus of *Pseudomonas aeruginosa*. J Bacteriol. 2005;187(6):2138–2147. doi: 10.1128/JB.187.6.2138-2147.2005

[46] Cornelis P, Dingemans J. *Pseudomonas aeruginosa* adapts its iron uptake strategies in function of the type of infections. Front Cell Infect Microbiol. 2013;3:75. doi: 10.3389/fcimb.2013.00075

[47] Ravel J, Cornelis P. Genomics of pyoverdine-mediated iron uptake in pseudomonads. Trends Microbiol. 2003;11(5):195–200. doi: 10.1016/S0966-842X(03)00076-3

[48] Kuhn ML, Majorek KA, Minor W, et al. Broad-substrate screen as a tool to identify substrates for bacterial Gcn5-related N-acetyltransferases with unknown substrate specificity. Protein Sci. 2013;22(2):222–230. doi: 10.1002/pro.2199

[49] Song Y, Zhang S, Ye Z, et al. The novel type II toxin-antitoxin PacTA modulates *Pseudomonas aeruginosa* iron homeostasis by obstructing the DNA-binding activity of Fur. Nucleic Acids Res. 2022;50(18):10586–10600.

[50] Kaneko Y, Thoendel M, Olakanmi O, et al. The transition metal gallium disrupts *Pseudomonas aeruginosa* iron metabolism and has antimicrobial and antibiofilm activity. J Clin Invest. 2007;117(4):877–888. doi: 10.1172/JCI30783

[51] Zhai X, Reinhardt CJ, Malabanan MM, et al. Enzyme architecture: amino acid side-chains that function to optimize the basicity of the active site glutamate of triosephosphate isomerase. J Am Chem Soc. 2018;140(26):8277–8286. doi: 10.1021/jacs.8b04367

[52] Vatansever C. Evolutionary adaptations in iron capture via type II pyoverdine in XDR *Pseudomonas aeruginosa*. Dataset. ST235_v2. figshare. 2026. doi: 10.6084/m9.figshare.31347037.v1

[53] Vatansever C. Raw sequencing and metadata associated with *Pseudomonas aeruginosa* ST235 isolates [dataset]. NCBI Bio Project. 2026. Accession: PRJNA1241513. https://www.ncbi.nlm.nih.gov/bioproject/PRJNA1241513